PCCP

PAPER

View Article Online
View Journal | View Issue

Cite this: *Phys. Chem. Chem. Phys.*, 2018, **20**, 17071

CO_2 adsorption on gas-phase $Cu_{4-x}Pt_x$ (x = 0–4) clusters: a DFT study†

Luis E. Gálvez-González,[a] J. Octavio Juárez-Sánchez,[b] Rafael Pacheco-Contreras,[b] Ignacio L. Garzón,[c] Lauro Oliver Paz-Borbón [c] and Alvaro Posada-Amarillas *[b]

Received 3rd February 2018,
Accepted 24th May 2018

DOI: 10.1039/c8cp00818c

rsc.li/pccp

Transition and noble metal clusters have proven to be critical novel materials, potentially offering major advantages over conventional catalysts in a range of value-added catalytic processess such as carbon dioxide transformation to methanol. In this work, a systematic computational study of CO_2 adsorption on gas-phase $Cu_{4-x}Pt_x$ (x = 0–4) clusters is performed. An exhaustive potential energy surface exploration is initially performed using our recent density functional theory basin-hopping global optimization implementation. Ground-state and low-lying energy isomers are identified for $Cu_{4-x}Pt_x$ clusters. Secondly, a CO_2 molecule adsorption process is analyzed on the ground-state $Cu_{4-x}Pt_x$ configurations, as a function of cluster composition. Our results show that the gas-phase linear CO_2 molecule is deformed upon adsorption, with its bend angle varying from about 132° to 139°. $Cu_{4-x}Pt_x$ cluster geometries remain unchanged after CO_2 adsorption, with the exception of Cu_3Pt_1 and Pt_4 clusters. For these particular cases, a structural conversion between the ground-state geometry and the corresponding first isomer configurations is found to be assisted by the CO_2 adsorption. For all clusters, the energy barriers between the ground-state and first isomer structures are explored. Our calculated CO_2 adsorption energies are found to be larger for Pt-rich clusters, exhibiting a volcano-type plot. The overall effect of a hybrid functional including dispersion forces is also discussed.

1. Introduction

One of the current important topics in materials science is the development of new and more efficient materials to form part of the renewable fuels production process,[1] in which conventional catalysts play a central role.[2–4] This has motivated studies of conversion of carbon dioxide (CO_2) to methanol (CH_3OH) and hydrocarbons such as methane (CH_4),[5,6] leading to exploration of an enormous variety of catalytic materials mostly based on transition and noble metals. However, the thermal and kinetic stabilities of CO_2 represent issues for conventional catalysts, which affect their performance toward transformation into value-added chemicals. Therefore, unconventional (nanoscaled), novel, and more efficient catalysts need to be developed,[7] thus the analysis of the interplay of molecules such as CO_2 with atomic clusters is becoming important.[8] These studies are overall relevant since the chemical fixation of these molecules is an important step in the production of renewable fuels through CO_2 transformation. Consequently, the trapping and activation of CO_2 have become topics of primary importance in present day research.

Transition and noble metal-based catalysts are among the most studied systems for CO_2 conversion reactions into methanol,[1,6,9] due in part to the relative stability of these metal catalysts under reaction conditions, and also, to the synergistic intermetallic effects that result from the combination of different metal elements.[10,11] These effects cause an enhacement of the chemical reactivity of nanoparticles and clusters, in which size and chemical ordering also play a significant role.[10,12] Control of these variables, together with the experimentally chosen CO_2 reduction route,[13] make the search for the best catalyst (for a specific reaction) laborious and exhaustive work. Therefore, in the past few years, research efforts have been focused on multimetallic nanometric catalysts and, in this regard, several recent review articles make reference to the different synthesis methods that have been developed for the transformation of CO_2 into useful chemicals.[6,13–17]

On the experimental side, numerous studies have shown the importance of nanoparticle size and composition, as well as the support, in the catalytic performance of pure and mixed

[a] *Programa de Doctorado en Ciencias (Física), División de Ciencias Exactas y Naturales, Universidad de Sonora, Blvd. Luis Encinas & Rosales, 83000, Hermosillo, Mexico*
[b] *Departamento de Investigación en Física, Universidad de Sonora, Blvd. Luis Encinas & Rosales, 83000 Hermosillo, Sonora, Mexico. E-mail: posada@cifus.uson.mx*
[c] *Instituto de Física, Universidad Nacional Autónoma de México, Apdo. Postal 20-364, 01000 Cd. de México, Mexico*

† Electronic supplementary information (ESI) available. See DOI: 10.1039/c8cp00818c

(alloyed) clusters and nanoparticles.[18–21] Particularly, size-selected (free and supported in alumina) copper clusters have been thoroughly studied to understand the differences in catalytic activity in the process of methanol synthesis from CO_2.[19] It is shown in that work that, in gas-phase clusters, there is a tendency revealing that activity increases as cluster size decreases, and that for supported clusters, the best performance in methanol production is obtained for the Cu_4/Al_2O_3 system. Likewise, several heterogeneous catalysts based on transition metals (Fe-, Cu-, and Ni-based) have proven to be more practical for industrial applications compared to homogeneous catalysts.[1,16] These data, together with other experimental studies indicating that copper is the best cathode for CO_2 conversion to CH_4,[16] suggest that copper-based catalysts are good candidates for advanced energy materials. In this sense, the prediction of the catalytic behavior has gained support through indices that have been proposed empirically, such as the Sabatier principle. For example, the activity volcano plot[22] has been used as a prediction tool, an approach that is based on the adsorption energy values of adsorbate molecules[23] and which partially aids in the systematic prediction of better catalysts.[24,25]

Theoretically, a number of investigations have been dedicated to understand, in detail, the structure and stability of mono and bimetallic clusters usually employing density functional theory (DFT).[25–29] Also, several attempts have been made to computationally design the best catalysts combining information on measured properties and calculated descriptors.[30] However, this is a complex task due to the multiple variables to be taken into account in the rational design of catalysts, and may lead to controversial outcomes. For instance, in quite recent studies, the role of the d-band center has been stressed as a descriptor of the catalytic activity of Ni-based alloy catalysts supported on alumina for CO_2 transformation to methane.[20] In that work, the d-density of states (d-DOS) is explored as a new descriptor to characterize the catalytic activity. Based on this, it was concluded that the $Ni–Fe/Al_2O_3$ alloy performs better than the corresponding $Ni–Cu/Al_2O_3$ catalyst. This result suggests a revision of copper as a potential strong catalyst as mentioned in ref. 19, where is indicated that the higher activity corresponds to the alumina-supported Cu_4 cluster as compared to the larger one. Another possibility[20] is that the alloy of Ni and Fe atoms performs better than that of Ni and Cu in promoting the catalytic activity to transform CO_2. And furthermore, the catalytic performance of the two alloys may be a consequence of the interaction of metal clusters with the support. The former suggests the necessity of further systematic theoretical studies given that the mechanisms involved in CO_2 adsorption and activation by metal clusters are not entirely understood. Due to structural stability playing a key role in the catalytic performance of metal clusters, a study on the behavior of the binding energy is also necessary as well as of diverse fragmentation pathways.

Recent experimental and computational studies on the utilization of supported subnanometric clusters for CO_2 activation[31–33] have stimulated, in this work, a thorough computational DFT study on the adsorption properties of CO_2 on $Cu_{4-x}Pt_x$ (x = 0–4) gas-phase clusters. It is motivated due to their relevance for the catalytic conversion of carbon dioxide (CO_2) to methanol (CH_3OH), and because bimetallic catalysts usually perform better that their monatomic counterparts. To this end, we first theoretically obtain ground-state and isomer structures of mono- and bimetallic Cu–Pt clusters through an *ab initio* global optimization procedure using the generalized gradient approximation (GGA) Perdew–Burke–Ernzerhof (PBE) functional.[34] The global search procedure used here has proven to be reliable to identify real minima and transition state structures.[35] The interaction of ground-state structures with one adsorbed CO_2 molecule is then studied, and dissociation channels are obtained for the ground state systems for bare clusters. The case of the Pt_4 cluster is analyzed separately under the PBE/SDD scheme, because of the existence of a structural transformation between the ground-state and first isomer structures as an effect of CO_2 adsorption. Thus, the approximate energy barrier to transformation is calculated to gain insight into the fluxional properties of the bare Pt_4 cluster. In our results, structural conversion behavior is also exhibited by the Cu_3Pt_1 cluster.

2. Theoretical and computational methodologies

The potential energy surface (PES) exploration of $Cu_{4-x}Pt_x$ clusters is carried out using our recent density functional theory global optimization implementation based on the basin hopping algorithm.[35–37] The PBE exchange–correlation functional is used,[34] along with the triple-ζ Stuttgart–Dresden (SDD) basis set,[38] under the DFT implementation of the Gaussian 09 package.[39] For each $Cu_{4-x}Pt_x$ cluster, different topological regions of the PES are reached by applying the ''shake'' and ''swap'' move classes to the cluster's coordinates. A maximal random displacement of 1.0 Å is used in the shake move, on each of the *xyz* atomic coordinates; while atom swapping only operates on bimetallic clusters due to the existence of homotop structures.[40] The Berny optimization procedure is repeated until convergence conditions on both forces ($<3.0 \times 10^{-4}$ Hartree per Bohr) and displacements ($<2.0 \times 10^{-3}$ Bohr) as well as their root mean square values, are reached. Initial configurations are randomly generated and 150 BH-DFT steps are carried out with no structural restrictions made during the global optimization procedure. Adsorption on bridge, top, and hollow cluster sites was also explored. The reported results correspond to the adsorption sites with the lowest total energy. In order to confirm ground-state configurations, the cluster's vibrational frequencies are calculated at the PBE/SDD level of theory. The effect of van der Waals (vdW) forces on the optimized cluster + CO_2 systems is assessed, using the long-range hybrid ωB97X-D functional.[41] For the optimization of the combined system (CO_2 + cluster), CO_2 was located on several sites on the ground state configurations of the metal clusters to search for the lowest energy final structures reported in this work. To validate the reliability of the PBE/SDD scheme on the

bare tetramer cluster energetic results, single-point calculations with two different functionals (M06-L[42] and M06[43]) using the def2-TZVPP basis set, were carried out to compare the relative energy of low-lying isomers with respect to the ground state structure. PBE/def2-TZVPP calculations were also performed to elucidate the effect of the basis set. Both M06-L and M06 functionals are based on the same analytical form, differing in the parameter values and the amount of Hartree–Fock exchange (0 and 27%, respectively).[43]

3. Energy analysis

For $Cu_{4-x}Pt_x$ clusters, their binding energy per atom (E_b) is monitored to examine the effect of alloying. It is calculated as:

$$E_b = -\frac{[E(Cu_{4-x}Pt_x) - (4-x)E(Cu) - xE(Pt)]}{4} \quad (1)$$

where x = 0–4. In this equation, E(Cu) and E(Pt) represent the calculated total energies of the Cu and Pt atoms, respectively, while $E(Cu_{4-x}Pt_x)$ is the total energy of the tetranuclear system. Additional information on the relative stability of bare clusters can be obtained by analyzing the influence of composition on the clusters' dissociation process. With this in mind, different possible fragmentation pathways, relevant under experimental conditions, are explored by computing the corresponding fragmentation energy ($\Delta E_{n,m}$):

$$\Delta E_{n,m} = E_m + E_{n-m} - E_n \quad (2)$$

where the terms of eqn (2) represent the difference between the total energy of the tetramer cluster (n) and its corresponding fragments: m and $n - m$, with ($n \geq m$).[44] The smaller the $\Delta E_{n,m}$ value, the stronger the preference for a particular fragmentation path. Furthermore, the linear synchronous transit (LST) method[45] is used to calculate the energy barrier between the 3D (T_d symmetry) ground-state (GS) and the first low-energy bent rhombus isomer (ISO1) geometries of the Pt_4 cluster, as we observe a structural transformation promoted by CO_2 adsorption. CO_2 adsorption energies (E_{ads}) on $Cu_{4-x}Pt_x$ clusters are calculated as total energy differences between the combined system (E_{total}), and the relaxed configurations of the metal cluster ($E_{cluster}$) and the gas-phase ($E_{adsorbate}$) CO_2 molecule:

$$E_{ads} = E_{cluster} + E_{adsorbate} - E_{total} \quad (3)$$

where positive values indicate a stronger interaction between the metal cluster and the CO_2 molecule.

4. Results and discussion

4.1 $Cu_{4-x}Pt_x$ bare clusters

Metal cluster structure conversion has been reported in direct imaging experiments where nuclearity is reasonably well-controlled.[46] Theoretically, global optimization algorithms have been developed to explore the potential energy surface (PES) of these clusters, yielding information about the ground-state structure and low-lying energy isomers. For the $Cu_{4-x}Pt_x$ gas-phase clusters, Fig. 1 shows their corresponding ground-state (GS) configurations at each composition, as well as isomer structures found within an energy window ranging from 0.05 up to 0.51 eV above the calculated GS energy.

From Fig. 1, one can observe that small energy differences are calculated for the Cu_4 cluster between the rhombus GS and the distorted ISO structures (+0.345 up to +0.368 eV). This is mostly due to a reduction in the number of Cu–Cu bonds, from 5 in the GS structure to 4 in the ISO configurations. Our GS configurations are in agreement with recent work on Pt–Cu gas-phase clusters.[47] For the bimetallic Cu_3Pt_1 case, the planarity of the rhombus configuration is preserved, though it is now slightly bent due to the presence of a Pt atom. However, a transition from the quasi-planar (GS) configuration to a full 3D geometry is predicted due to a small (+0.062 eV) energy difference. The small energy difference between these two structures can be rationalized by a d-orbital directionality effect from the Pt atom, as in both cases the number of three Pt–Cu bonds is maintained. A larger energy penalty is calculated when the number of Pt–Cu and Cu–Cu bonds is reduced (ISO2 and ISO3 structures), compared to the GS configuration. As the number of Pt atoms is increased, such as in Cu_2Pt_2, Cu_1Pt_3 and Pt_4 clusters, the maximization of the number of Pt–Pt bonds becomes clear for the GS structures, as the corresponding GS structures become 3D (T_d symmetry).

We investigated the accuracy of the relative energies predicted by the PBE/SDD scheme (SC1) shown in Fig. 1, comparing the performance with that of the M06-L and M06 functionals combined with the def2-TZVPP basis set (SC3 and SC4, respectively). The results shown in Table 1 indicate that the different approaches present discrepancies in the relative energies, still showing a similar tendency when considering each cluster's isomers. However, the M06-L functional allow a slightly better discrimination of the energy difference between bimetallic Cu_3Pt_1 isomers and a good performance for those of the Pt_4 cluster. PBE/def2-TZVPP performs better for the Pt_4 cluster, whereas the Cu_4 cluster is well described by all the functionals employed in this work. Calculations using the PBE/def2-TZVPP scheme (SC2) have been performed to account for polarization in the basis set.

Overall, the disagreement of the calculated values between functionals may be attributed to both the basis set and the physical basis underlying the respective functional form. The M06-L and M06 functionals contain different parameter values but have a similar functional form, self-interaction correction, and terms associated with the Laplacian of the electron density, $n(r)$; besides, M06 is a global hybrid functional containing 27% Hartree–Fock exchange, which is not present in the M06-L functional. The GGA PBE functional is nonempirical and depends only on $n(r)$ and $\nabla n(r)$. The results in Table 1 indicate that the PBE functional is reliable to perform DFT calculations on this type of mono- and bimetallic clusters.

Interestingly, for Pt_4, a quasi-planar bent rhombus (2D) structure is only +0.174 eV higher in energy, both structures having 5 Pt–Pt bonds. Previous work on DFT-based global optimization has also reported a 3D (T_d symmetry) structure as a putative GS configuration,[48] while in recent work using a

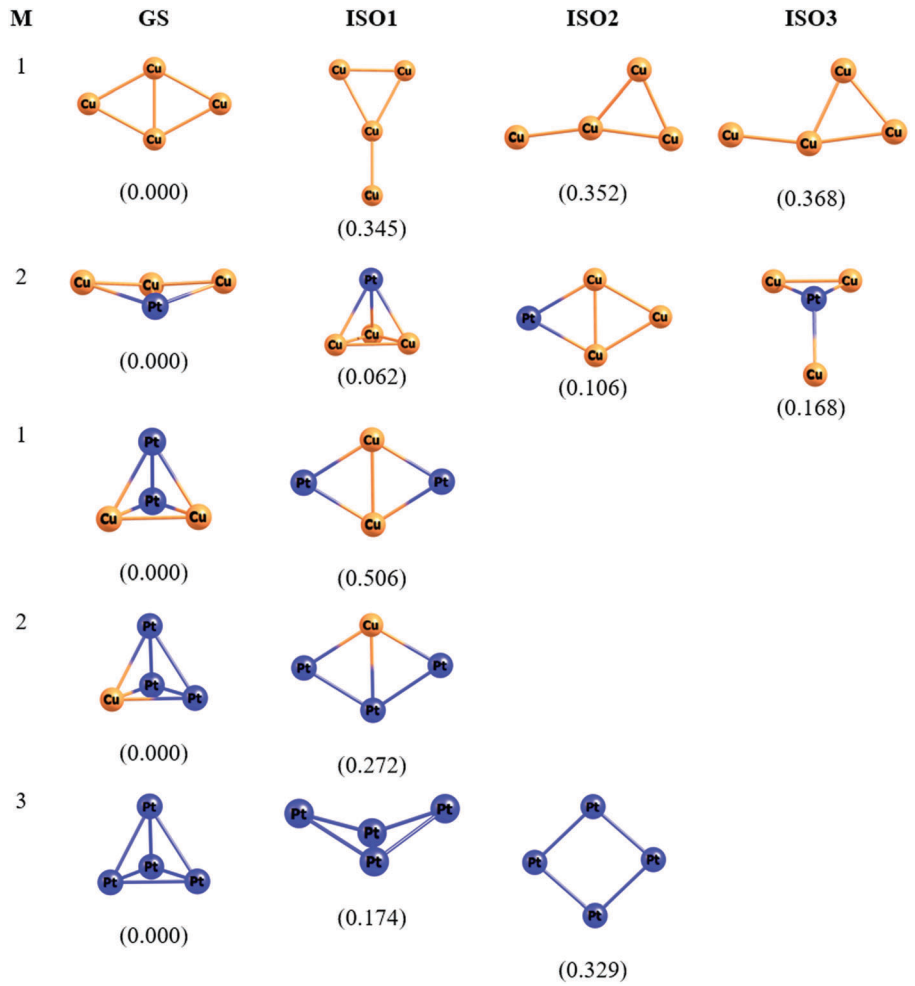

Fig. 1 Ground-state (GS) and low-lying isomer (ISO) structures of $Cu_{4-x}Pt_x$ (x = 0–4) gas-phase clusters. The corresponding multiplicity (M = 2S + 1) is also shown. Numbers in parentheses indicate the energy difference between the GS geometry and the corresponding low-lying isomer in eV.

Table 1 Relative energies (ΔE in eV) calculated using the DFT approaches PBE/SDD (SC1), PBE/def2-TZVPP (SC2), M06-L/def2-TZVPP (SC3), and M06/def2-TZVPP (SC4). The percentage change between neighboring isomers in the same column, shown in parenthesis, is calculated through $[(\Delta E\_ISO_{i+1} - \Delta E\_ISO_i)/\Delta E\_ISO_{i+1}] \times 100$

Cluster	Isomer	SC1	SC2	SC3	SC4
Cu_4	ISO1	0.345	0.407	0.467	0.344
	ISO2	0.352 (2%)	0.410 (1%)	0.472 (1%)	0.348 (1%)
	ISO3	0.368 (4%)	0.416 (1%)	0.488 (3%)	0.359 (3%)
Cu_3Pt_1	ISO1	0.062	0.060	0.060	0.201
	ISO2	0.106 (41%)	0.145 (59%)	0.233 (74%)	0.305 (34%)
	ISO3	0.168 (37%)	0.234 (38%)	0.401 (42%)	0.328 (7%)
Cu_2Pt_2	ISO1	0.506	0.569	0.728	0.837
Cu_1Pt_3	ISO1	0.272	0.156	0.470	0.757
Pt_4	ISO1	0.174	0.031	0.231	0.158
	ISO2	0.329 (47%)	0.159 (80%)	0.507 (54%)	0.435 (64%)

DFT periodic approach, we reported a pseudo 2D bent rhombus as a putative GS configuration highlighting intrinsic differences between using plane-waves and gaussian-type orbitals,[29] as well as previous theoretical work.[47] Either way, structural interconversion is possible if the transition energy barrier is low, implying a relatively flat PES. Further information on the binding energy (E_b), the average first neighbor distances ($\langle d \rangle$), and the minimum and maximum value of vibrational frequencies (ω) for the ground-state and first isomer structures of $Cu_{4-x}Pt_x$ (x = 0–4) gas-phase clusters is given in Table 2.

In general, calculated E_b values and average distances ($\langle d \rangle$) change almost linearly with the chemical composition, with larger values calculated as the number of Pt atoms increases, reaching a maximum at the monometallic Pt_4 cluster. Finally, positive vibrational frequencies (ω) indicate that both GS and ISO1 configurations are local minima of the cluster PES and do not correspond to a transition state. For the ground-state Cu_3Pt_1 cluster, the ω_{min} frequency corresponds to a symmetric bending mode.

4.2 Cluster fragmentation pathways

To gain additional insight into the stability properties of the GS structures, a cluster fragmentation analysis is performed.

Table 2 Structural and energetic properties of gas-phase tetramer Cu–Pt clusters. The minimum and maximum values of harmonic frequencies are also shown

Cluster	$\langle d \rangle$ (Å)	E_b (eV per atom)	ω_{min} (cm^{-1})	ω_{max} (cm^{-1})
Cu_4 (GS)	**2.370**	**1.503**	**59.146**	**269.905**
Cu_4 (ISO1)	2.336	1.416	19.362	294.806
Cu_3Pt_1 (GS)	**2.426**	**1.908**	**25.846**	**250.508**
Cu_3Pt_1 (ISO1)	2.438	1.893	86.556	268.725
Cu_2Pt_2 (GS)	**2.508**	**2.374**	**90.363**	**257.649**
Cu_2Pt_2 (ISO1)	2.427	2.247	39.436	258.938
Cu_1Pt_3 (GS)	**2.566**	**2.719**	**100.048**	**243.030**
Cu_1Pt_3 (ISO1)	2.501	2.651	37.355	228.468
Pt_4 (GS)	**2.636**	**2.994**	**80.545**	**213.017**
Pt_4 (ISO1)	2.569	2.950	25.868	204.730

The corresponding fragmentation energy ($\Delta E_{n,m}$) is calculated along with the possible fragmentation pathways for the largest clusters considered, such as monometallic Cu_4 and bimetallic Cu_3Pt_1. $\Delta E_{n,m}$ is defined as the energy needed to dissociate a (neutral) n-size atom cluster into fragmented clusters composed of m and $(n - m)$ atoms, with larger fragmentation energies indicating superior cluster stability. For the pure metal GS tetramer Cu_4 and Pt_4 clusters, two possible dissociation channels are calculated:

$$\mathbf{Cu_4 \rightarrow Cu_2 + Cu_2 \quad \Delta E_{2,2} = 1.672\ eV}$$

$$\rightarrow Cu_3 + Cu_1 \quad \Delta E_{3,1} = 2.567\ eV$$

$$\mathbf{Pt_4 \rightarrow Pt_2 + Pt_2 \quad \Delta E_{2,2} = 3.517\ eV}$$

$$\rightarrow Pt_3 + Pt_1 \quad \Delta E_{3,1} = 3.886\ eV$$

For both cases, the larger $\Delta E_{n,m}$ values suggest that fission is not favored by initially evaporating one atom out of the tetramer. A small $\sim$0.37 eV ($\sim$8 kcal mol^{-1}) energy difference in fragmentation energy for the Pt_4 cluster suggests a competition between the two possible processes. Thus, the abundance of stable Pt dimers is expected to be similar to that of the Pt trimers. For the Cu_4 cluster, this difference increases to nearly 0.9 eV ($\sim$21 kcal mol^{-1}), indicating that the most probable fragmentation process for neutral Cu_4 corresponds to the evaporation of two copper atoms (stable dimers). Our results differ from cationic copper cluster results in collision induced dissociation experiments.[49] No experimental information was found in the literature for neutral Cu clusters. Thus, in order to have theoretically predicted results able to be compared with those in ref. 49, the dissociation channels of Cu_4^+ and Cu_3^+ clusters were explored. It was found that, in agreement with the experimental results, the energetically favorable processes correspond to (a) the loss of a neutral atom for the Cu_4 cation, and (b) the loss of a neutral dimer for the Cu_3^+ cluster, as shown in the following simulated fragmentation processes:

$$\mathbf{Cu_4^+ \rightarrow Cu_3^+ + Cu_1 \quad \Delta E_{3,1} = 1.724\ eV}$$

$$\rightarrow Cu_2^+ + Cu_2 \quad \Delta E_{2,2} = 2.977\ eV$$

$$\mathbf{Cu_3^+ \rightarrow Cu_1^+ + Cu_2 \quad \Delta E_{1,2} = 3.533\ eV}$$

$$\rightarrow Cu_1^+ + 2Cu_1 \quad \Delta E_{1,1} = 5.704\ eV$$

Analysis of the bimetallic cluster fission process is slightly more complex due to the increase in the number of possible fragmentation channels. For Cu_3Pt_1 and Cu_1Pt_3 GS structures, three processes are analyzed, as shown below:

$$\mathbf{Cu_3Pt_1 \rightarrow Cu_2Pt_1 + Cu_1 \quad \Delta E_{2\text{-}1,1} = 2.020\ eV}$$

$$\rightarrow Cu_2 + Cu_1Pt_1 \quad \Delta E_{1\text{-}1,2} = 2.386\ eV$$

$$\rightarrow Cu_3 + Pt_1 \quad \Delta E_{3,1} = 4.187\ eV$$

and

$$\mathbf{Cu_1Pt_3 \rightarrow Pt_3 + Cu_1 \quad \Delta E_{3,1} = 2.786\ eV}$$

$$\rightarrow Pt_2 + Cu_1Pt_1 \quad \Delta E_{1\text{-}1,2} = 3.570\ eV$$

$$\rightarrow Cu_1Pt_2 + Pt_1 \quad \Delta E_{2,2} = 4.030\ eV$$

while four dissociation processes are possible in the case of the Cu_2Pt_2 cluster:

$$\mathbf{Cu_2Pt_2 \rightarrow Cu_1Pt_2 + Cu_1 \quad \Delta E_{1\text{-}2,1} = 2.650\ eV}$$

$$\rightarrow Cu_2 + Pt_2 \quad \Delta E_{2,2} = 3.097\ eV$$

$$\rightarrow Cu_1Pt_1 + Cu_1Pt_1 \quad \Delta E_{1\text{-}1,1\text{-}1} = 3.343\ eV$$

$$\rightarrow Cu_2Pt_1 + Pt_1 \quad \Delta E_{2\text{-}1,1} = 3.883\ eV$$

Overall, our calculations indicate that for all the bimetallic clusters considered, fragmentation is energetically favored by first evaporating a single Cu atom over Cu–Pt or Pt–Pt dimer units, in line with the chemical bond strength Cu–Cu < Cu–Pt < Pt–Pt. This implies that in all cases, removal of one Pt atom is energetically the costliest fragmentation pathway.

4.3 Clusters with adsorbate

Fig. 2 shows the final configuration of the adsorbed CO_2 molecule on the ground state structures of Cu–Pt clusters, for all compositions. Interestingly, this figure shows isomerization upon adsorption for clusters Cu_3Pt_1 and Pt_4. In the latter case, earlier studies[50] did not show this structural conversion, which will be analyzed later in this work through an analysis of the energy barriers to isomerization in bare clusters.

For all involved clusters, an apparent bend in the CO_2 molecule is observed upon relaxation, which causes an increase in its reactivity.[4,51] This bend is explained as a result of the electron density transference to the LUMO in the process of stabilization.[52] In our study, to verify whether this mechanism is valid for all clusters, we plotted (Fig. 3) the cluster + CO_2

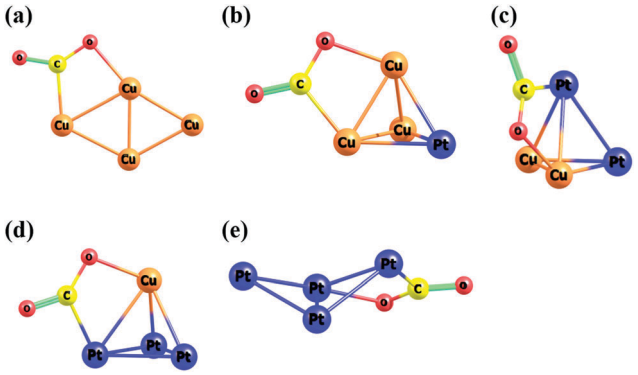

Fig. 2 The lowest-energy configurations of CO_2 adsorbed on (a) Cu_4, (b) Cu_3Pt_1, (c) Cu_2Pt_2, (d) Cu_1Pt_3, and (e) Pt_4 gas-phase clusters.

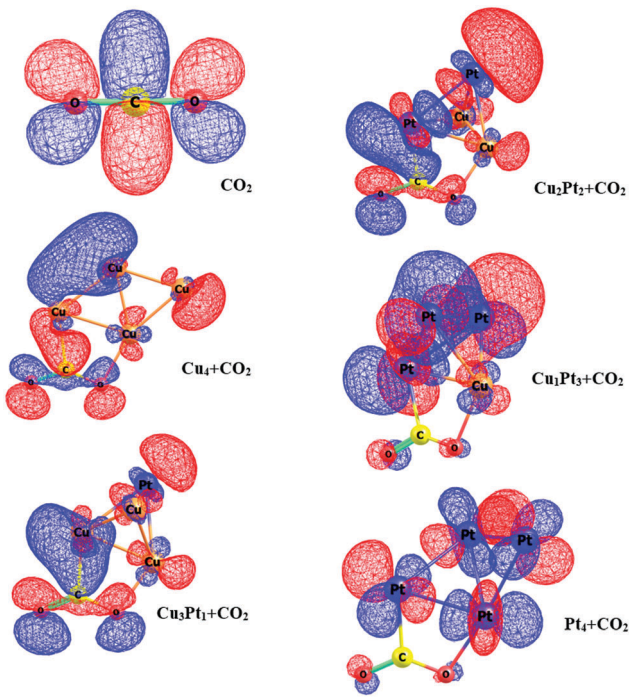

Fig. 3 Plot of the LUMO orbital for each of the clusters in this study. In Pt-rich clusters, electron density is highly localized on each metal atom, and is small and localized on the oxygen atoms of the bent CO_2 molecule.

LUMO frontier orbitals and, as a reference, the corresponding LUMO of the linear CO_2 molecule.

In this figure, it is apparent that the charge transfer mechanism explains the stabilization of CO_2 in the majority of the studied cases, basically Cu-rich clusters, which are known to be selective in CO_2 transformation into CH_3OH.[53] However, for the Pt-rich clusters Cu_1Pt_3 and Pt_4, charge transfer is not observed toward the CO_2 LUMO, which barely exhibits electron density localized on the oxygen atoms. This may explain the poor performance of Pt-based catalysts for CO_2 activation.[54]

Our calculations also indicate that the bridge site is the preferred position for CO_2 adsorption. For bimetallic clusters, except Cu_3Pt_1, the CO_2 molecule is bound to the metal cluster *via* its C–O in a bridge position between the Cu and Pt atoms,

Table 3 Calculated HOMO–LUMO gap (E_g), adsorption energies (E_{ads}, in eV), cluster average distances ($\langle d \rangle$) and each homogeneous ($\langle d_{Pt-Pt} \rangle$, $\langle d_{Cu-Cu} \rangle$) and heterogeneous ($\langle d_{Pt-Cu} \rangle$) bond of $Cu_{4-x}Pt_x$ (x = 0–4) gas-phase clusters. Calculations involving both PBE and dispersion-corrected (ωB97X-D) functionals are shown for adsorbed CO_2 molecule configurations

Cluster		E_g (eV)	E_{ads} (eV)	$\langle d \rangle$ (Å)	$\langle d_{Cu-Cu} \rangle$ (Å)	$\langle d_{Pt-Cu} \rangle$ (Å)	$\langle d_{Pt-Pt} \rangle$ (Å)
Cu_4	Bare	0.981	—	2.370	2.370	—	—
	+Ads(PBE)	1.003	0.807	2.402	2.402	—	—
	+Ads(ωB97XD)	6.176	3.020	2.365	2.365	—	—
Cu_3Pt_1	Bare	0.466	—	2.426	2.408	2.439	—
	+Ads(PBE)	0.495	1.013	2.473	2.491	2.455	—
	+Ads(ωB97XD)	4.622	2.985	2.450	2.405	2.480	—
Cu_2Pt_2	Bare	0.640	—	2.508	2.511	2.478	2.627
	+Ads(PBE)	1.044	1.644	2.544	2.549	2.525	2.617
	+Ads(ωB97XD)	6.544	3.928	2.575	2.631	2.553	2.606
Cu_1Pt_3	Bare	0.477	—	2.567	—	2.528	2.605
	+Ads(PBE)	0.280	1.444	2.601	—	2.598	2.603
	+Ads(ωB97XD)	5.880	3.634	2.624	—	2.648	2.599
Pt_4	Bare	0.134	—	2.636	—	—	2.636
	+Ads(PBE)	0.269	1.158	2.583	—	—	2.583
	+Ads(ωB97XD)	5.391	3.093	2.583	—	—	2.583

with the C atom always binding to a Pt atom. A comparison of the energetical and structural parameters between pure clusters and clusters with adsorbate is given in Table 3. For most of the clusters, the calculated adsorption energy is larger than 1 eV, except for the Cu_4 cluster onto which the CO_2 adsorption strength is ~0.8 eV using the PBE functional. Interestingly, this value compares quite well with that obtained by Liem and Clarke[55] (0.751 eV) for a bent CO_2 molecule adsorbed on the Cu(110) surface.

From Fig. 4, one can observe that the weakest E_{ads} value corresponds to the CO_2 molecule adsorbed on the Cu_4 cluster, while the strongest E_{ads} value is calculated for the CO_2 molecule on the bimetallic Cu_2Pt_2 cluster. The E_{ads} values decrease when we reach the full monometallic Pt_4 cluster. This resembles a volcano-type plot as a function of Cu_xPt_{4-x} cluster composition,

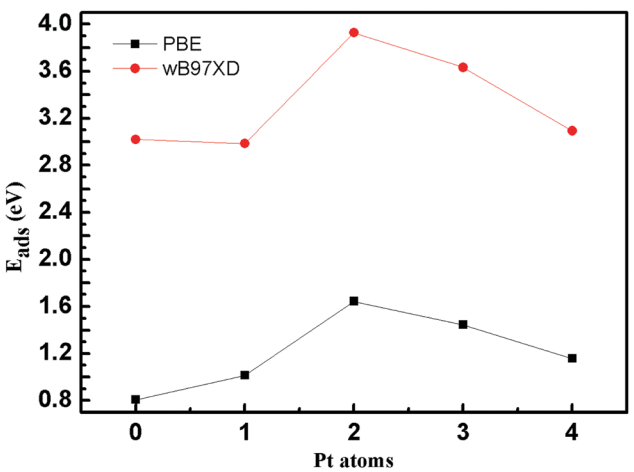

Fig. 4 Calculated E_{ads} values of CO_2 on Cu_xPt_{4-x} (x = 0–4) gas-phase clusters, using both PBE and the dispersion corrected ωB97X-D exchange–correlation functional.

for both functionals. From Table 3, an analysis of the average distance for the bare clusters shows that for pure clusters, it increases almost linearly as the number of Pt atoms increases; a tendency that prevails in the PBE calculated lattice constant of bulk Pt (3.92 Å) compared to the Cu one (3.64 Å).[56,57] When the CO_2 molecule is adsorbed, the average distance behavior shows slightly larger values when dispersion effects are included (no more than 1.6%), compared to the PBE functional, in agreement with previous studies on the applicability of hybrid functionals to small metal clusters.[58]

Overall, one can observe that the calculated structural properties are barely affected by either the GGA or the hybrid functional used. However, the use of a hybrid functional has a significant impact because rather large E_{ads} values and HOMO–LUMO gaps (E_g) are calculated in this work, when empirical atom–atom dispersion corrections are included *via* the long range corrected hybrid ωB97X-D functional[59] (see Table 3). This seems to be an artifact likely due to the ωB97X-D functional parametrization – for atoms and molecules – and the inclusion of 100% long-range exact-exchange. It has been previously reported that the use of Hartree–Fock exchange within the hybrid functional badly affects small metal clusters, as it produces a depleted DOS near the Fermi level leading to a widening of the HOMO–LUMO gap. It has also been demonstrated that, in PBE-based functionals, combining dispersion interaction with nonlocal corrections overestimates the adsorption energy.[60] However, the trend in adsorption may remain unchanged, for example as was demonstrated for adsorption of O_2 on MgO-supported Pt–Ni clusters.[61] Thus, an inaccurate description of their electronic structure may be expected for the small metal clusters in this study.[41,62,63] Following the above consideration, only results obtained using the PBE functional are discussed for CO_2 adsorption on the metal clusters.

When CO_2 is interacting with the metal clusters, the molecule bends (see Fig. 2). For Cu-rich clusters, this is due to a charge transfer process toward the CO_2 molecule that leads to the formation of a more reactive $CO_2^{\delta-}$ anion, as our NBO charge analysis corroborates (see Table 4).[4,64] Our results show that upon adsorption, the O–C–O angle slowly decreases, while the average C–O distance increases. It is noteworthy that the amount of electron density transferred from the cluster to the molecule is necessary to provide structural stability to the combined system configuration. It is possible to assess the energetic cost to CO_2 structural distortion by performing a thorough study of the distortion energy. This can be realized by taking the energy difference between the relaxed cluster + bent molecule and the relaxed cluster + (frozen) linear molecule configurations;[65] however, this would go beyond the purview of this investigation. Catalytic activity and selectivity investigations are still necessary to elucidate which of the studied clusters is the best candidate for a specific chemical reaction, and to what extent the amount of charge transferred contributes in modifying the reactivity properties of the bent CO_2 molecule.[51]

Finally, our computational outcomes show the existence of structural conversion induced by CO_2 adsorption, reached at clusters Cu_3Pt_1 and Pt_4 under the PBE/SDD scheme. This peculiar behavior justifies the analysis of the PES flatness associated with these metal clusters. To this end, the linear synchronous transit (LST) method is used to calculate, firstly, the Pt_4 and Cu_3Pt_1 clusters' geometrical transformation from their ground-state (GS) to the first isomer (ISO1) leading to a sensitive estimation of the transition state (TS) energy barrier.

Table 4 Structural details of the CO_2 molecule illustrating the effect of cluster composition on the C–O distance (d_{C-O}) and its average value ($\langle d_{C-O}\rangle$), both in Å, and the bend angle value (in degrees). The last column shows the total natural charge for each cluster after molecule adsorption

	$\langle d_{C-O}\rangle$ (Å)	∠ O–C–O	δ^+
Linear	1.206	180.0	—
Cu_4	1.274	138.6	0.483
Cu_3Pt_1	1.291	132.5	0.591
Cu_2Pt_2	1.287	136.6	0.463
Cu_1Pt_3	1.284	137.2	0.446
Pt_4	1.289	134.3	0.409

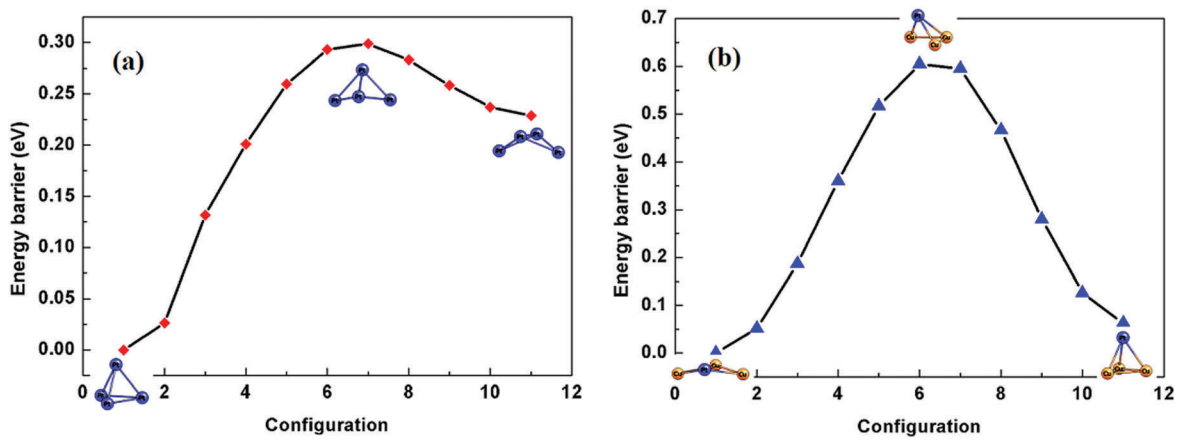

Fig. 5 Transition state energy barriers calculated using the linear synchronous transit (LST) method between (a) the 3D pyramidal ground-state (GS) geometry Pt_4 cluster and (b) the quasi-planar GS configuration Cu_3Pt_1 cluster, and their corresponding first isomer (ISO1) structures. The transition state structures are shown at the top of the energy barriers.

Fig. 5(a and b) exhibits the energy landscape details between the initial, transition state, and final structures, for both Pt_4 and Cu_3Pt_1. For both, the fragmentation energy of the most favorable route to fragmentation is larger than the theoretical estimate of the activation energy shown here.

For Pt_4, the TS barrier is rather small, with a calculated value of 0.30 eV, clearly demonstrating the fluxional character of the Pt_4 cluster assisted *via* CO_2 interaction. For the Cu_3Pt_1 cluster the estimated activation energy resulted to be about 0.60 eV, twice that of the Pt_4 cluster.

This predicted structural conversion behavior stimulates the search for a correlation between the calculated energy barrier between the ground-state and first isomer structures and the cluster's chemical composition. Thus, we have also calculated the energy barrier for clusters that do not undergo a structural conversion before CO_2 adsorption, namely the Cu_4, Cu_1Pt_3 and Cu_2Pt_2 clusters (see Fig. S1(a–c) in ESI†). The estimated value of the barrier height is about 0.64, 1.33 and 1.07 eV, respectively. For bimetallic clusters, it is apparent that on increasing the number of Pt atoms, the barrier height also increases, following the tendency $Cu_3Pt_1 < Cu_2Pt_2 < Cu_1Pt_3$. At this point, it is noteworthy to mention that the characteristics of the calculated energy barrier are related to the amount of correlation energy, as was stated by Espinosa-Garcia *et al.*,[66] which might explain the slight difference between the barrier height of clusters Cu_4 (monometallic) and Cu_3Pt_1 (bimetallic). This consideration may be important in the computational study of Cu-based clusters participating in chemical reaction processes.

5. Conclusions

In this work we have reported a systematic study on CO_2 adsorption on $Cu_{4-x}Pt_x$ clusters. Using a BH-DFT global optimization algorithm we initially located the ground-state and low-lying energy isomers for $Cu_{4-x}Pt_x$ clusters. Then, the adsorption process of one CO_2 molecule is analyzed on the calculated ground-state cluster configurations, as a function of cluster composition. Our results indicate a rather strong interaction between the CO_2 molecule and metal clusters, with E_{ads} values ranging from 0.806 eV up to 1.644 eV, reaching a maximum value on the bimetallic Cu_2Pt_2 cluster, thus resembling a volcano-type plot. Upon adsorption, CO_2 undergoes a geometric deformation, changing from a linear configuration to a bent one, with the O–C–O angle varying from about 132° to 139°. $Cu_{4-x}Pt_x$ cluster geometries remain unchanged after CO_2 adsorption, with the exception of the Cu_3Pt_1 and Pt_4 clusters. For these, the interaction with the CO_2 molecule causes a drastic structural change in the original geometries, leading to a final configuration where these clusters have been transformed into the corresponding first isomer configuration. Interestingly, a charge transfer mechanism to the LUMO orbital explains the CO_2 bend[52] for Cu-rich clusters. Further analysis is necessary in order to understand the CO_2 adsorption process in Pt-rich clusters. Our calculated CO_2 adsorption energies are found to be larger for Pt-rich clusters, exhibiting a volcano-type plot.

In this study, the CO_2 interaction is observed to cause a structural conversion in the Cu_3Pt_1 and Pt_4 clusters due to a rather small (0.60 and 0.30 eV, respectively) transition state energy barrier between the ground state and the first low-lying cluster geometries. From a theoretical point of view, the Cu_3Pt_1 cluster may be a good candidate as a heterogeneous ultra-small nanocatalyst, because the ground state structure activates the CO_2 molecule upon adsorption; secondly, as shown in Table 3, the adsorption energy lies in the range of energies indicated for optimal catalysts, according to the Sabatier principle; and thirdly, because under the appropriate experimental conditions, cluster structural reversibility can be switched on and off. Additionally, our computational results on $Cu_{4-x}Pt_x$ cluster fragmentation indicate that a cluster dissociation mechanism is not possible before a reversible structural transformation due to the large fragmentation energy needed (>2 eV). The barrier height changes with composition in bimetallic clusters, following a trend $Cu_3Pt_1 < Cu_2Pt_2 < Cu_1Pt_3$.

Our results also indicate that although the structural properties of these clusters are correctly described by a long range corrected hybrid ωB97X-D (dispersion-corrected) functional – compared to a GGA (PBE) one – it leads to a poor description of the metal cluster electronic structure combined with a strong overestimation of the CO_2 adsorption energy values. Finally, further theoretical and experimental studies are needed in order to gain a deeper insight into the catalytic activity and selectivity properties of these subnanometer mono- and bimetallic clusters, both in the gas-phase and supported over oxide surfaces.

Conflicts of interest

The authors declare that there are no conflicts of interest regarding the publication of this article.

Acknowledgements

APA is grateful to Dr Dora J. Borbón-González for helpful discussions on the reliability of functionals, and Conacyt-México for financial support through project grant No. 180424. LOPB and ILG are thankful for the financial support from the Universidad Nacional Autónoma de México, Dirección General Asuntos del Personal Académico (DGAPA-UNAM), under Projects IA102716 and IN108817, as well as cpu-time from Supercómputo UNAM (Miztli) through DGTIC-UNAM LANCAD-UNAM-DGTIC-307 grants.

References

1 W. Wang, S. Wang, X. Ma and J. Gong, *Chem. Soc. Rev.*, 2011, **40**, 3703–3727.
2 J. Wambach, G. Illing and H.-J. Freund, *Chem. Phys. Lett.*, 1991, **184**, 239–244.
3 F. Solymosi, *J. Mol. Catal.*, 1991, **65**, 337–358.

4 H.-J. Freund and M. W. Roberts, *Surf. Sci. Rep.*, 1996, **25**, 225–273.
5 O. K. Varghese, M. Paulose, T. J. LaTempa and C. A. Grimes, *Nano Lett.*, 2009, **9**, 731–737.
6 P. G. Jessop, T. Ikariya and R. Noyori, *Chem. Rev.*, 1995, **95**, 259–272.
7 R. Psaro, C. Dossi, R. Della Pergola, L. Garlaschelli, S. Calmotti, S. Marengo, M. Bellatreccia and R. Zanoni, *Appl. Catal., A*, 1995, **121**, L19–L23.
8 S. A. Ruatta, P. A. Hintz and S. L. Anderson, *J. Chem. Phys.*, 1991, **94**, 2833–2847.
9 S. Vukojevic, O. Trapp, J.-D. Grunwaldt, C. Kiener and F. Schüth, *Angew. Chem., Int. Ed.*, 2005, **44**, 7978–7981.
10 D. Bazin, D. Guillaume, Ch. Pichon, D. Uzio and S. Lopez, *Oil Gas Sci. Technol.*, 2005, **60**, 801–813.
11 D. Wang, A. Villa, F. Porta, L. Prati and D. Su, *J. Phys. Chem. C*, 2008, **112**, 8617–8622.
12 R. Ferrando, J. Jellinek and R. L. Johnston, *Chem. Rev.*, 2008, **108**, 845–910.
13 G. Zhao, X. Huang, X. Wang and Xi. Wang, *J. Mater. Chem. A*, 2017, **5**, 21625–21649.
14 T. Sakakura, J.-C. Choi and H. Yasuda, *Chem. Rev.*, 2007, **107**, 2365–2387.
15 H. Zhou and X. Lu, *Sci. China: Chem.*, 2017, **60**, 904–911.
16 Y. Li, S. H. Chan and Q. Sun, *Nanoscale*, 2015, **7**, 8663–8683.
17 Y. Attia and M. Samer, *Renewable Sustainable Energy Rev.*, 2017, **79**, 878–892.
18 M. D. Porosoff and J. G. Chen, *J. Catal.*, 2013, **301**, 30–37.
19 B. Yang, C. Liu, A. Halder, E. C. Tyo, A. B. F. Martinson, S. Seifert, P. Zapol, L. A. Curtiss and S. Vajda, *J. Phys. Chem. C*, 2017, **121**, 10406–10412.
20 K. Ray and G. Deo, *Appl. Catal., B*, 2017, **218**, 525–537.
21 C. Liu, B. Yang, E. Tyo, S. Seifert, J. DeBartolo, B. von Issendorf, P. Zapol, S. Vajda and L. A. Curtiss, *J. Am. Chem. Soc.*, 2015, **137**, 8676–8679.
22 C. J. H. Jacobsen, S. D. Bjerne, S. Clausen, S. Bahn, A. Loggadotir and J. K. Nørskov, *J. Am. Chem. Soc.*, 2001, **123**, 8404–8405.
23 A. B. Anderson, *Electrocatalysis*, 2012, **3**, 176–182.
24 F. Calle-Vallejo, M. D. Pohl, D. Reinish, D. Loffreda, P. Sautet and A. S. Bandarenka, *Chem. Sci.*, 2017, **8**, 2283–2289.
25 N. Shan, M. Zhou, M. K. Hanchett, J. Chen and B. Liu, *Mol. Simul.*, 2017, **43**, 861–885.
26 D. F. Mukhamedzyanova, N. K. Ratmanova, D. A. Pichugina and N. E. Kuz'menko, *J. Phys. Chem. C*, 2012, **116**, 11507–11518.
27 S. Darby, T. V. Mortimer-Jones, R. L. Johnston and C. Roberts, *J. Chem. Phys.*, 2002, **116**, 1536–1550.
28 D. J. Borbón-González, A. Fortunelli, G. Barcaro, L. Sementa, R. L. Johnston and A. Posada-Amarillas, *J. Phys. Chem. A*, 2013, **117**, 14261–14266.
29 L. O. Paz-Borbón, A. López-Martínez, I. L. Garzón, A. Posada-Amarillas and H. Grönbeck, *Phys. Chem. Chem. Phys.*, 2017, **19**, 17845–17855.
30 M. P. Andersson, T. Bligaard, A. Kustov, K. E. Larsen, J. Greeley, T. Johannessen, C. H. Christensen and J. K. Nørskov, *J. Catal.*, 2006, **239**, 501–506.
31 M. Qiu, H. Tao, Y. Li, Y. Li, K. Ding, X. Huang, W. Chen and Y. Zhang, *Appl. Surf. Sci.*, 2018, **427**, 837–847.
32 X. Zhao, B. Luo, R. Long, C. Wang and Y. Xiong, *J. Mater. Chem. A*, 2015, **3**, 4134–4138.
33 K. Yang and B. Yang, *Phys. Chem. Chem. Phys.*, 2017, **19**, 18010–18017.
34 J. P. Perdew, K. Burke and M. Ernzerhof, *Phys. Rev. Lett.*, 1996, **77**, 3865–3868.
35 J. C. Luque-Ceballos, A. Posada-Borbón, R. Herrera-Urbina, R. Aceves, J. O. Juárez-Sánchez and A. Posada-Amarillas, *Physica E*, 2018, **97**, 1–7.
36 Z. Li and H. A. Scheraga, *Proc. Natl. Acad. Sci. U. S. A.*, 1987, **84**, 6611–6615.
37 D. J. Wales and J. P. K. Doye, *J. Phys. Chem. A*, 1997, **101**, 5111–5116.
38 M. Dolg and X. Cao, *Chem. Rev.*, 2012, **112**, 403–480.
39 M. J. Frisch, G. W. Trucks, H. B. Schlegel, G. E. Scuseria, M. A. Robb, J. R. Cheeseman, G. Scalmani, V. Barone, B. Mennucci, G. A. Petersson, H. Nakatsuji, M. Caricato, X. Li, H. P. Hratchian, A. F. Izmaylov, J. Bloino, G. Zheng, J. L. Sonnenberg, M. Hada, M. Ehara, K. Toyota, R. Fukuda, J. Hasegawa, M. Ishida, T. Nakajima, Y. Honda, O. Kitao, H. Nakai, T. Vreven, J. A. Montgomery, Jr., J. E. Peralta, F. Ogliaro, M. Bearpark, J. J. Heyd, E. Brothers, K. N. Kudin, V. N. Staroverov, R. Kobayashi, J. Normand, K. Raghavachari, A. Rendell, J. C. Burant, S. S. Iyengar, J. Tomasi, M. Cossi, N. Rega, J. M. Millam, M. Klene, J. E. Knox, J. B. Cross, V. Bakken, C. Adamo, J. Jaramillo, R. Gomperts, R. E. Stratmann, O. Yazyev, A. J. Austin, R. Cammi, C. Pomelli, J. W. Ochterski, R. L. Martin, K. Morokuma, V. G. Zakrzewski, G. A. Voth, P. Salvador, J. J. Dannenberg, S. Dapprich, A. D. Daniels, Ö. Farkas, J. B. Foresman, J. V. Ortiz, J. Cioslowski and D. J. Fox, *Gaussian 09, Revision B.01*, Gaussian, Inc., Wallingford CT, 2009.
40 J. Jellinek and E. B. Krissinel, *Chem. Phys. Lett.*, 1996, **258**, 283–292.
41 J.-D. Chai and M. Head-Gordon, *Phys. Chem. Chem. Phys.*, 2008, **10**, 6615–6620.
42 Y. Zhao and D. G. Truhlar, *J. Chem. Phys.*, 2006, **125**, 194101.
43 Y. Zhao and D. G. Truhlar, *Theor. Chem. Acc.*, 2008, **120**, 215–241.
44 H. Yu, D. Cao, A. Fisher, R. L. Johnston and D. Cheng, *Appl. Surf. Sci.*, 2017, **396**, 539–546.
45 T. A. Halgren and W. N. Lipscomb, *Chem. Phys. Lett.*, 1977, **49**, 225–232.
46 Z. W. Wang and R. E. Palmer, *Nanoscale*, 2012, **4**, 4947–4949.
47 A. S. Chaves, G. G. Rondina, M. J. Piotrowski and J. L. F. Da Silva, *Comput. Mater. Sci.*, 2015, **98**, 278–286.
48 A. Trinchero, S. Klacar, L. O. Paz-Borbón, A. Hellman and H. Grönbeck, *J. Phys. Chem. C*, 2015, **119**, 10797–10803.
49 O. Ingólfsson, U. Busolt and K.-i. Sugawara, *J. Chem. Phys.*, 2000, **112**, 4613–4620.

50 C. Liu, H. He, P. Zapol and L. A. Curtiss, *Phys. Chem. Chem. Phys.*, 2014, **16**, 26584–26599.
51 S. K. Iyemperumal and N. A. Deskins, *Phys. Chem. Chem. Phys.*, 2017, **19**, 28788–28807.
52 Y.-G. Wang, K. B. Wiberg and N. H. Werstiuk, *J. Phys. Chem. A*, 2007, **111**, 3592–3601.
53 Y. Yang, J. Evans, J. A. Rodriguez, M. G. White and P. Liu, *Phys. Chem. Chem. Phys.*, 2010, **12**, 9909–9917.
54 S. Kattel, B. Yan, J. G. Chen and P. Liu, *J. Catal.*, 2016, **343**, 115–126.
55 S. Y. Liem and J. H. R. Clarke, *J. Chem. Phys.*, 2004, **121**, 4339–4345.
56 A. Kokalj and M. Causà, *J. Phys.: Condens. Matter*, 1999, **11**, 7463–7480.
57 A. Soon, M. M. Todorova, B. Delley and C. Stampfl, *Phys. Rev. B: Condens. Matter Mater. Phys.*, 2007, **75**, 125420.
58 T. M. Soini, A. Genest, A. Nikodem and N. Rösch, *J. Chem. Theory Comput.*, 2014, **10**, 4408–4416.
59 J.-D. Chai and M. Head-Gordon, *Phys. Chem. Chem. Phys.*, 2008, **10**, 6615–6620.
60 J. Girgis and B. G. Janesko, *Theor. Chem. Acc.*, 2013, **132**, 1335.
61 L. O. Paz-Borbón and F. Baletto, *Inorganics*, 2017, **5**, 43.
62 W. Gao, T. A. Abtew, T. Cai, Y.-Y. Sun, S. Zhang and P. Zhang, *Solid State Commun.*, 2016, **234–235**, 10–13.
63 J. Paier, M. Marsman and G. Kresse, *J. Chem. Phys.*, 2007, **127**, 024103.
64 W. Taifan, J.-F. Boily and J. Baltrusaitis, *Surf. Sci. Rep.*, 2016, **71**, 595–671.
65 L. O. Paz-Borbón, R. L. Johnston, G. Barcaro and A. Fortunelli, *Eur. Phys. J. D*, 2009, **52**, 131–134.
66 J. Espinosa-Garcia, S. Tolosa and J. C. Corchado, *J. Phys. Chem.*, 1994, **98**, 2337–2340.

